First comprehensive particle balance study in KSTAR with a full graphite first wall and diverted plasmas

2012 Plasma Phys. Control. Fusion 54 105006

(http://iopscience.iop.org/0741-3335/54/10/105006)

Plasma Phys. Control. Fusion **54** (2012) 105006 (13pp) doi:10.1088/0741-3335/54/10/105006

First comprehensive particle balance study in KSTAR with a full graphite first wall and diverted plasmas

Yaowei Yu[1,2], Suk-Ho Hong[1,3,4,5,6], Si-Woo Yoon[1], Kwang-Pyo Kim[1], Woong-Chae Kim[1], Jae-Min Park[1], Young-Suk Oh[3], Hoon-Kyun Na[1], Jun-Gyo Bak[1], Kyu-Sun Chung[3] and the KSTAR Team

[1] National Fusion Research Institute, Daejeon, 305-806, Korea
[2] Institute of Plasma Physics, Chinese Academy of Sciences, PO Box 1126, Hefei, Anhui 230031, People's Republic of China
[3] Department of electrical engineering, HanYang University, Seoul, 133-791, Korea
[4] Center for Edge Plasma Science (cEps), HanYang University, Seoul, 133-791, Korea
[5] University of Science and Technology, Daejeon, 305-333, Korea

E-mail: sukhhong@nfri.re.kr and yuyaowei@ipp.ac.cn

Received 10 April 2012, in final form 12 July 2012
Published 31 August 2012
Online at stacks.iop.org/PPCF/54/105006

Abstract
The first comprehensive particle balance study is carried out in the KSTAR 2010 campaign with a full graphite first wall and diverted plasmas. The dominant retention is observed during the gas puffing into the plasmas. Statistical analysis shows that deuterium retention is increased with the number of injected particles. Particle balance analysis in the whole campaign shows that the long-term retention ratio is ∼21%, and the retention via implantation can be partially recovered by He-glow discharge cleaning (GDC), while long-term retention via co-deposition. The wall pumping capability is decreased with the D_2 plasma due to fuel accumulation in the first wall, and He-GDC is effective in recovering the wall pumping. Boronization assisted by the D_2 glow discharge using $C_2B_{10}H_{12}$ strongly enhances the wall puffing and leads to negative retentions, but the wall pumping capability is recovered in 2–3 days by He-GDCs. Electron cyclotron resonance heating enhances wall outgassing during the discharge. During a diverted H-mode discharge, the retention rate decreases to a very low value, and a high divertor particle flux of $\sim 1.5 \times 10^{23}\,\mathrm{D\,s^{-1}}$ is observed indicating the strong recycling divertor. The amount of recovered deuterium after discharges mainly depends on the plasma–wall interaction when the plasma is terminated, and disruptive discharges release more particles from the first wall.

(Some figures may appear in colour only in the online journal)

1. Introduction

Fuel retention is one of the crucial points to be investigated for fusion devices [1–3], and particle balance is a reliable method for the study. Fuel retention affects fuelling efficiency, plasma density control and the density of neutral hydrogenic particles in the plasma boundary, which in turn affects particle and energy confinement [1]. Furthermore, excessive tritium accumulation in the first wall will induce a safety problem for next-generation tokamak operation, for instance, the maximum tolerable tritium mass of ITER in-vessel inventory is limited to 700 g [1, 3, 4].

There are two main fuel retention mechanisms, implantation and co-deposition [4]. The implantation depth is limited by incident particle energies and the first wall temperature. Implantation is significant in short-pulse discharges [1] and the wall surface will be saturated by the continuous incidence of hydrogenic particles. Once the surface is saturated, wall pumping capability can be recovered by means of thermal release, ion-induced release and isotope

[6] Author to whom any correspondence should be addressed.

exchange, corresponding to disruptive discharges, helium discharges and hydrogenic discharges, respectively. But for retention via co-deposition, a-C : H(D) layer can grow continuously throughout the discharge, thus it can trap fuel particles indefinitely with a continuous retention rate [2, 5], unless the co-deposition layer is eroded by the plasma, or flaked into dust mainly due to the layer thickness limit [1]. This process is considered to be responsible for the long-term retention, and oxidation (with the first wall at a temperature of > 570 K or assisted by an oxygen plasma discharge) may be an effective and feasible way to remove fuel particles in co-deposited layers with both laboratory and tokamak experiences [1, 4, 6].

Fuel retention studies in current tokamaks could establish good techniques and database for ITER, and particle balance study is a high priority task compared with post-mortem analysis [7]. Global particle balance analysis is popularly used in different tokamaks: both short-term and long-term retention are obtained, which are beneficial to investigate the retention mechanisms and the influence of different plasma parameters as reported below. From the TRIAM-1M's 11 406 s long discharge without active cooling of plasma-facing components (PFC), it was observed that the retention behaviors in discharges with continuous gas feed and with additional gas puffing were different, and the maximum wall inventory was $\sim 3.6 \times 10^{20}$ H atoms in 30 min. However, most of the injected particles were released from the wall at the end of the discharge due to the temperature increase over the whole toroidal area of the main chamber [8]. But in Tore Supra with active cooling of PFCs there was no saturation observed during a 6 min long-pulse and high-power (totally 1 GJ) discharge, and the retained particles increased with time, indicating that the outgassing with active cooling PFCs was well controlled [2, 9]. JT-60U has also found that during 30 s of an edge localized mode (ELMy) discharge, the wall characteristic was gradually changed from pumping to puffing, which was caused by an increase in the tile temperature around the outer strike point [10]. In DIII-D, time-dependent particle balance analysis of H-mode discharges indicates that major fuel retention has occurred during the initial ohmic and L-mode phase of the discharges, with a peak fuel retention rate of $\sim 2 \times 10^{21}$ D s^{-1} (D-atoms/s), but decreased to almost zero during the later stationary phase of the discharge [5]. A detailed analysis of the static and dynamic balance provided an estimation of the global co-deposition rate of $\leqslant (0.6\text{–}1.2) \times 10^{20}$ D s^{-1} [5]. The result on MAST showed that fuel retention was almost 100% (short-pulse discharges, <1 s), but most of the retained particles could be recovered by inter-shot He-glow discharge cleaning (GDC), and disruptions could also reduce the wall inventory [11]. In JET, disruptive discharges release approximately two times more particles than non-disruptive discharges [12]. Fuel retention with carbon and tungsten first wall materials was compared in ASDEX Upgrade (AUG) and it was observed that the retention on carbon walls seemed to be higher than that on non-boronized tungsten walls [13]. Particle balance analysis in carbon-dominated tokamaks (TEXTOR, AUG, Tore Supra and JET) showed that retention rates were from ~ 1 g D h^{-1} (8.4×10^{19} D s^{-1}) in TEXTOR, up to $\sim$6–12 g D h^{-1} ($(5\text{–}10) \times 10^{20}$ D s^{-1}) in AUG (during the 2002–2003 campaign when AUG was a carbon-dominated machine), but it could reach $\sim$10–25 g D h^{-1} ($(8.4\text{–}20.9) \times 10^{20}$ D s^{-1}) in JET and $\sim$15–40 g D h^{-1} ($(1.3\text{–}3.3) \times 10^{21}$ D s^{-1}) in AUG in high-performance discharges [14].

In the Korea Superconducting Tokamak Advanced Research (KSTAR) 2010 campaign, particle balance analysis is employed to study fuel retention with a full graphite first wall. Deuterium retention is evaluated by global particle balance analysis. A typical retention evolution during a discharge is analyzed. The effect of He-GDC and boronization assisted by a D_2 glow discharge is investigated. The retention behavior is studied in different parameter plasmas, including diverted H-mode, electron cyclotron resonant heating (ECRH), disruptive and non-disruptive discharges. Moreover, the correlation between the retention rate and the discharge pulse length is discussed. This study provides significant support for the future KSTAR operation especially on plasma density control and wall conditioning to recover the retained fuel. In addition, the results will be valuable for future superconducting tokamaks like ITER.

2. Experimental set-up and methods

2.1. KSTAR and main parameters

KSTAR is a superconducting tokamak with a minor radius of $a = 0.5$ m and major radius of $R = 1.8$ m; it has single and double-null diverted plasma configurations [15]. The first wall is covered by graphite tiles with an area of 1.5 m^2 in 2008, 11 m^2 in 2009, and a complete graphite wall of 54 m^2 with a passive stabilizer in the 2010 campaign, including the limiter and divertor regions, and the sum of the upper and lower divertor areas is $\sim$21.5–25.8 m^2 in different shaped plasmas. The total volume of the vacuum vessel including all ports is $\sim$110 m^3, and the plasma volume is in the range 7–16 m^3 depending on the shape of the plasmas, which is estimated from EFIT by taking the last closed flux surface (LCFS) as the plasma edge. No PFC was actively cooled in the KSTAR 2010 campaign, therefore the wall temperature is initially around at room temperature in the morning and it is increased with discharges (see figure 8 as an example). A schematic diagram of KSTAR is given in figure 1, including the vacuum vessel pumping system, the ECRH system, the ion cyclotron resonant heating (ICRH) system, the neutral beam injection (NBI) system and the boronization system. Main diagnostics are a millimeter-wave interferometer, H-alpha (H_α/D_α), electron cyclotron emission (ECE), a bolometer array, hard x-ray, an x-ray imaging crystal spectrometer (XICS), charge-exchange spectroscopy (CES), a fast reciprocating Langmuir probe (FRP), an edge probe array (poloidal position is shown in figure 10) and so on.

In the KSTAR 2010 campaign, the magnetic field (B_T) is usually set at 2.0 T with the maximum value of 3.2 T. Both circular and diverted plasmas, with a maximum plasma current (I_p) ~ 0.7 MA and average line density up to 4.5×10^{19} m^{-3}, are obtained with ohmic and auxiliary heating. For diverted discharges, the duration of the initial ramp-up phase is 1–2 s,

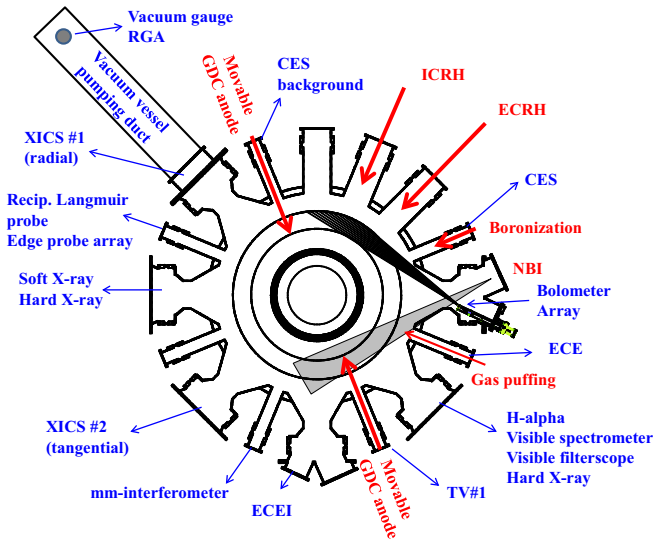

Figure 1. Top view of the KSTAR layout in the 2010 campaign, including particle balance relevant systems, main diagnostics, heating systems and wall conditioning systems.

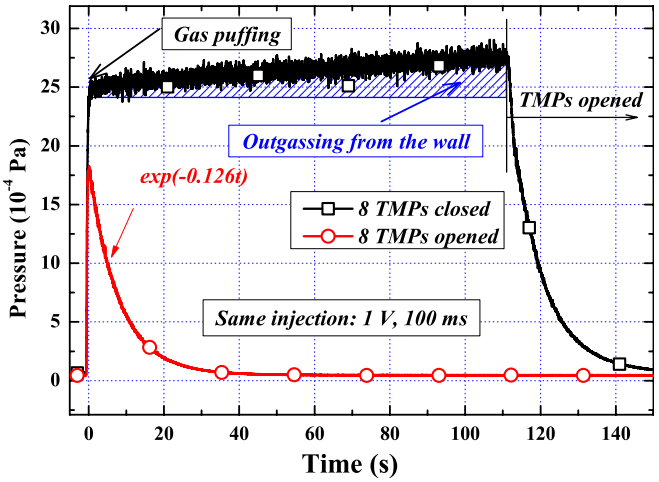

Figure 2. Calibration of piezoelectric valve and pumping speed, neutral pressure evolution with gas puffing via piezoelectric valve, 1 V and 100 ms, squares (□) are for the pressure when all pumps are closed before gas puffing and opened ∼110 s later, and circles (○) are for the pressure when eight TMPs are always open. The shaded area shows the wall outgassing.

and the diverted phase is in the consequent 1–4 s. ECRH is used, both 84 and 110 GHz gyrotrons, with a capability of 500 kW for plasma start-up and heating. 500 kW ICRH is used at a frequency of 40 MHz and $B_T = 2$ T. Moreover, NBI with a beam energy of 70–90 keV and an injected power of up to 1.4 MW is employed, with a maximum injection duration of 2.7 s (longer duration of 3 s at lower power of 1.2 MW). H-mode is achieved with $I_p = 0.6$ MA, $B_T = 2.0$ T, in a well-balanced double-null configuration after the boronization wall with an additional heating power of 1.4 MW NBI and 0.2 MW ECRH [15]. The typical edge plasma parameters are measured by FRP: electron temperature (T_e) ∼ 20–60 eV, electron density (n_e) ∼ (8–25) × 10^{17} m^{-3} [16].

During the KSTAR 2010 campaign, He-GDC is routinely employed at night and early morning to remove retained deuterium and other impurities between run days. The morning He-GDC is carried out for ∼1 h, and after that there are usually 1.5–2 h vacuum pumping before the plasma experiment, which is useful for helium pumping out from the first wall. Therefore, the amount of He retained in the first wall by He-GDC is considered to be low enough, and the He fraction is neglected in the particle balance calculation. Boronization using a D_2 glow discharge and $C_2B_{10}H_{12}$ is carried out two times during the experiment to remove impurities and to control the H fraction in the boron film. Since no inter-shot wall conditioning is used, fuel retention of each day is simply monitored by the balance of daily gas injection and exhaustion. Totally ∼804 plasma shots with $I_p > 100$ kA and pulse length >0.3 s are performed in 44 run days, and the longest pulse is 6.7 s. The total plasma duration of these shots is 2898 s, in which ∼780 s are divertor plasmas, and the rest are limiter plasmas; the total duration of H-mode is very short, ∼19 s. The deuterium retention during D_2 boronization or D_2 GDC is not measured and thus not included in the particle balance, therefore the retention should be concentrated in the experiments before D_2 boronization. Before the first D_2 boronization, the total number of injected particles is 5.3×10^{23} D with an average injection of 8.2×10^{20} D/shot (2.2×10^{20} D s^{-1}), and the total number of particles pumped and removed by He-GDC is 4.2×10^{23} D, and long-term retention is 1.1×10^{23} D (∼21%), with the average long-term retention rate of 4.6×10^{19} D s^{-1}.

2.2. Gas injection and the pumping system

The vacuum vessel pumping duct of KSTAR has a circular cross-section of 1.4 m diameter, and it is connected to the KSTAR B port, as shown in figure 1. The length of the duct from the connection flange is 8 m, while the distance from the flange to the inside opening is 1.28 m. The conductance of the entire duct is about 32.4 m^3 s^{-1} for hydrogen [17]. Eight turbo molecular pumps (TMPs) and two cryo-pumps are installed on the pumping duct. All eight TMPs are used for discharge experiments, but only two or three are used for wall conditionings. The two cryo-pumps at the pumping duct are always closed during the discharges, and very seldom opened after the plasma is terminated, but soon closed again before the next shot. Upper and lower divertor cryo-pumps are installed, but not used in the KSTAR 2010 campaign. A cold cathode ionization gauge (PKR251) and a residual gas analyzer (RGA) are installed at the end of the pumping duct to monitor the neutral and partial pressures, and a piezoelectric valve is used for the gas puffing, as shown in figure 1.

The piezoelectric valve and effective pumping speed of the eight TMPs for deuterium are calibrated every year before the campaign [18]. An example of calibration data is shown in figure 2 with an applied voltage of 1 V and duration of 100 ms, and the gas puffing rate in KSTAR 2010 can be calculated by the applied voltage as follows:

$$\Gamma_{puff} = 10^{21} \times (0.4230 - 0.9368 \cdot V + 2.2398 \cdot V^2 - 0.4071 \cdot V^3), \quad (1)$$

where Γ_{puff} is the puffing rate in D s^{-1} and V is the imposed voltage of the piezoelectric valve in volts. The total effective

pumping speed of the eight TMPs for deuterium for the KSTAR vacuum vessel is $\sim$13.9 $m^3\,s^{-1}$, which is obtained from the fitting of the pressure curve by an exponential function, as shown in figure 2. The gradual increase in the pressure without pumping is due to the static wall outgassing ($\sim 2.5 \times 10^{-4}$ Pa $m^3\,s^{-1}$, major components are CO and CO_2 from the graphite wall, and this value would be lowered by continuous 10 days' wall conditioning before plasma experiments).

The pumping speed of the NBI system is changed with the pressure, in the range 14–26 $m^3\,s^{-1}$, which is obtained by the same method as for the TMPs. The pumping speed is affected by the variation of gas pressure (increasing with neutral pressure). Particle injection via the NBI system is evaluated by

$$\Gamma_{\mathrm{NBI}} = 6.25 \times 10^{21} \cdot P_{\mathrm{NBI}}/E_{\mathrm{f}} + \Gamma_0, \tag{2}$$

where P_{NBI} is the injected power of NBI in MW, E_{f} is the particle energy in keV and Γ_{NBI} is the injection rate in D s^{-1}. Furthermore, a small quantity of neutral deuterium from the NBI ion source chamber Γ_0 is also injected into the KSTAR vacuum vessel along with the NBI power injection; its average value is $\sim 7.7 \times 10^{18}$ D s^{-1}, which is obtained from the neutral pressure variation.

2.3. Particle balance evaluation

There is no cryogenic divertor pump used in the KSTAR 2010 campaign, and consequently particle balance can only be carried out by the number of particle injected subtracting the number of particle exhausted. The particle retention rate $\Gamma_{\mathrm{wall}}(t)$ is calculated in a shot by the particle balance [4, 19–21]

$$\Gamma_{\mathrm{wall}}(t) = \Gamma_{\mathrm{puff}}(t) + \Gamma_{\mathrm{NBI}}(t) - \left[Q_{\mathrm{pump}}(t) + \frac{\mathrm{d}N_{\mathrm{p}}(t)}{\mathrm{d}t} + \frac{\mathrm{d}N_0(t)}{\mathrm{d}t} \right], \tag{3}$$

where $Q_{\mathrm{pump}}(t)$ is the particle exhausting rate by pumps:

$$Q_{\mathrm{pump}}(t) = P_{\mathrm{duct}} \cdot S_{\mathrm{TMP}} + P_{\mathrm{NBI}} \cdot S_{\mathrm{NBI}}, \tag{4}$$

where P_{duct} and P_{NBI} are the neutral pressures of the pumping duct and the NBI chamber, S_{TMP} and S_{NBI} are the pumping speeds of the TMP and NBI cryo-panels, respectively. The amount of gas pumped out is the time integral of $Q_{\mathrm{pump}}(t)$. The typical time interval between two shots is 10–20 min, and two different integration times are used, (1) to compare the different plasma parameters' effect on fuel retention; the same duration of 600 s is used for all of the studied shots, and (2) to monitor the wall inventory evolution in one day; the time integration of $Q_{\mathrm{pump}}(t)$ is always continued from the first shot to the last shot of one day.

$N_{\mathrm{p}}(t)$ is the plasma inventory:

$$N_{\mathrm{p}}(t) = \frac{n_{\mathrm{e}}}{L_{\mathrm{chord}}} \times V_{\mathrm{plasma}}, \tag{5}$$

where n_{e} is the line integral density in $10^{19}\,m^{-2}$, L_{chord} is the chord length of mm-interferometer measurement in meter, V_{plasma} is the plasma volume in m^3. Both L_{chord} and V_{plasma} are calculated from EFIT.

$N_0(t)$ is the neutral particles in the vacuum vessel:

$$N_0(t) = P_{\mathrm{vessel}} \cdot (V_{\mathrm{vessel}} - V_{\mathrm{plasma}}) \tag{6}$$

$$P_{\mathrm{vessel}} = P_{\mathrm{duct}} \cdot \left(1 + \frac{S_{\mathrm{TMP}}}{U_{\mathrm{VD}}}\right) + \frac{\mathrm{d}P_{\mathrm{duct}}}{\mathrm{d}t} \cdot \frac{V_{\mathrm{duct}}}{U_{\mathrm{VD}}}, \tag{7}$$

where P_{vessel} is the neutral pressure of the vacuum vessel, and V_{vessel} is the vessel volume, 110 m^3. In KSTAR 2010 campaigns there is no direct measurement of neutral pressure in the vacuum vessel, while multi-chamber model analysis shows that P_{vessel} can be calculated by formula (7), where U_{VD} and V_{duct} are the conductance and volume of the pumping duct, respectively.

The error of gas puffing is $\sim$7% from the piezoelectric valve calibration, and that of the pumping speed of TMPs is $\sim$7%, the plasma inventory has an error of $\sim$10%, but the amount of gas injection is usually 2–5 times higher than the plasma inventory. Thus, the uncertainty of particle balance in shots without NBI could be evaluated as 9% for the retention rate during a discharge and 14% for total retention after the discharge. The injected particle by NBI has a large error due to the complex ingredients (D, D_2 and D_3) [5]. Nevertheless, this term (typically $\sim 10^{19}$ D s^{-1}) is much smaller than that of gas puffing (typically $\sim 10^{21}$ D s^{-1}), so the error of NBI could be neglected. The pumping speed of the NBI system for the main chamber has a large error of $\sim$20%, but the exhausted particles by the NBI system during the discharge is very small due to the short duration (<6.7 s) and very low neutral pressure. Therefore, the uncertainty of retention rate during the discharge is almost independent of the NBI system, but the total number of exhausted particles after a discharge has a larger uncertainty of $\sim$24%, and consequently an uncertainty of total retention of $\sim$31%.

3. Experimental results

3.1. Particle balance evolution during a discharge

A typical particle balance evolution of the circular limiter plasma is shown in figure 3. The time evolution of the shot can be divided into several phases, as the markers (1)–(7) in figure 3 between two adjacent red dashed lines:

(1) Plasma start-up: after the pre-filling, the plasma is started from the lower out-board side by the assistance of ECRH, and neutral particles are ionized into the plasma inventory. The retention rate increases as the plasma current increases at the initial phase, and then it varies quickly due to the ECRH heating (detailed analysis in section 3.4.2). The plasma then impacts the inner wall (see radial position (Rp-1.8) in figure 3(f)), and the wall retention increases slowly in $\sim$0.8 s and then remains almost constant in figure 3(e).

(2) Gas puffing into plasma: after the plasma start-up, the plasma inventory is increased almost linearly with time, with a constant gas puffing rate of 10^{21} D s^{-1} for 1 s. The increment of the plasma inventory is only $\sim$18% of the amount of additional gas puffing, and strong retention is observed in this phase with an average retention rate of

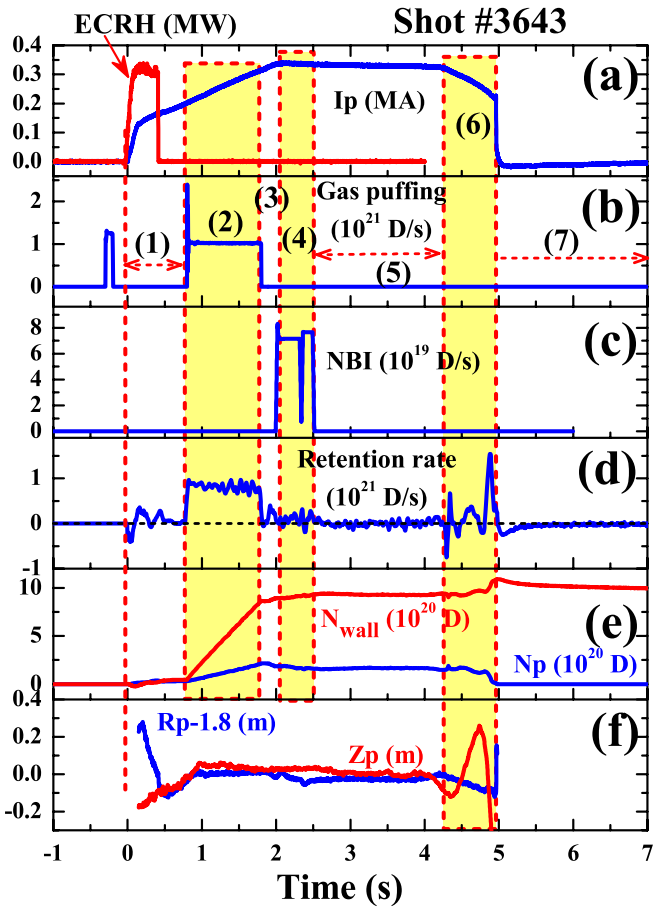

Figure 3. Time-dependent fuel retention of KSTAR shot #3643, (*a*) plasma current (I_p, blue) in MA and ECRH power in MW (red), (*b*) gas puffing rate in 10^{21} D s^{-1}, (*c*) particle injection rate by NBI in 10^{19} D s^{-1}, (*d*) retention rate in 10^{21} D s^{-1}, (*e*) plasma inventory (N_p, blue) and wall retention (N_{wall}, red) in 10^{20} D, and (*f*) plasma radial position (Rp-1.8) and vertical position Z_p.

8.2×10^{20} D s^{-1}, which is 82% of the gas puffing rate. This phase can be treated as the dominant phase for transient retention.

(3) Density decrease: after gas puffing stops, the density decreases gradually. The decay time depends on the particle confinement time and wall recycling. There is a slight increase in wall retention (from 8.6 to 8.9 $\times$ 10^{20} D) due to the particle loss to the first wall.

(4) NBI: after NBI is started with $E_f = 70$ keV, $P_{NBI} \sim 0.8$ MW, which is equivalent to a particle injection rate of 7.4×10^{19} D s^{-1}. The plasma inventory is increased slightly. But soon the increased heating power leads to a decrease in the particle confinement time; this causes another decrease in plasma inventory. In this phase, the average retention rate is 8.4×10^{19} D s^{-1}, which is even higher than the injection rate of NBI, but still ~10 times lower than that in additional gas puffing in phase (2).

(5) Natural density: after NBI is stopped, there is no additional gas injection. The plasma density is maintained by deuterium recycling from the first wall, and wall inventory is also constant. In this case, the plasma density is the so-called 'natural density' [2].

(6) Plasma ramp-down: as the current ramp-down begins, the plasma–surface interaction changes, which leads to a change in the wall retention rate instantaneously. Most of the plasma particles impact the first wall and temporarily stay on the wall surface. Part of them with high energy can even penetrate into the bulk of graphite [22]. As a consequence, the retention rate is increased, and at the end of the discharge there is a peak in the retention rate, as shown in figure 3(*d*).

(7) Exhausting after the plasma is terminated: after the plasma is terminated the first wall starts outgassing, thus a negative retention rate is observed. The number of recovered particles depends on the plasma condition at the ramp-down, mainly the plasma inventory, stored energy and quench rate of plasma energy.

During shot #3643, the total number of injected particles is 1.2×10^{21} D. The total number of particles pumped out during and after the discharge (600 s) is 3.9×10^{20} D, and 8.1×10^{20} D are retained in the first wall, i.e. the retention rate is ~68%. From figure 3 it is observed that the dominant retention occurs in the phase of particle injection into the plasma. Retention is also influenced by ECRH injection, plasmas impacting on the first wall and disruptions, which will be discussed in detail in the following sections.

3.2. Total fuel retention

The number of retained particles and retention fraction of discharges before and after the first D_2 boronization with plasma current >100 kA, and pulse length >0.3 s obtained using the particle balance are shown in figure 4. The plasma current decay time is defined as the '60% linear decay' time, which is the time required for a 60% drop of the pre-disruption plasma current, i.e. from 95% to 35% [23], and the plasma current quench rate is also calculated from this 60% decay. In this paper, shots with plasma current quench rate larger than 40 MA s^{-1} are considered as disruptive discharges, and those with less than 40 MA s^{-1} are considered as non-disruptive 'normal' discharges. It should be noted that most of the shots in 2010 are classified as disruptive because KSTAR did not employ any technique for soft landing. The criterion of 40 MA s^{-1} selected here has no physical meaning but only for the comparison of fuel retention in plasmas with different quench rates. In the KSTAR 2010 campaign, the term 'low gas injection' means that there is only a pre-filling before the plasma start-up and no further particle injection after that (the total number of injected particles $<8 \times 10^{19}$ D), while 'high gas injection' indicates there is additional gas puffing during the discharge (the total number of injected particles $>1.2 \times 10^{20}$ D).

It is observed in figure 4(*a*) that particle retention generally increases with the number of injected particles. Together with the retention rate in figure 3 it can be concluded that gas puffing has a strong effect on retention. Normal discharges show ~50–90% retention of injected particles with a small deviation. Fuel retention of disruptive discharges has lower values as reported from other machines [9, 10] and is scattered with a larger deviation. The deviation of disruptive discharges

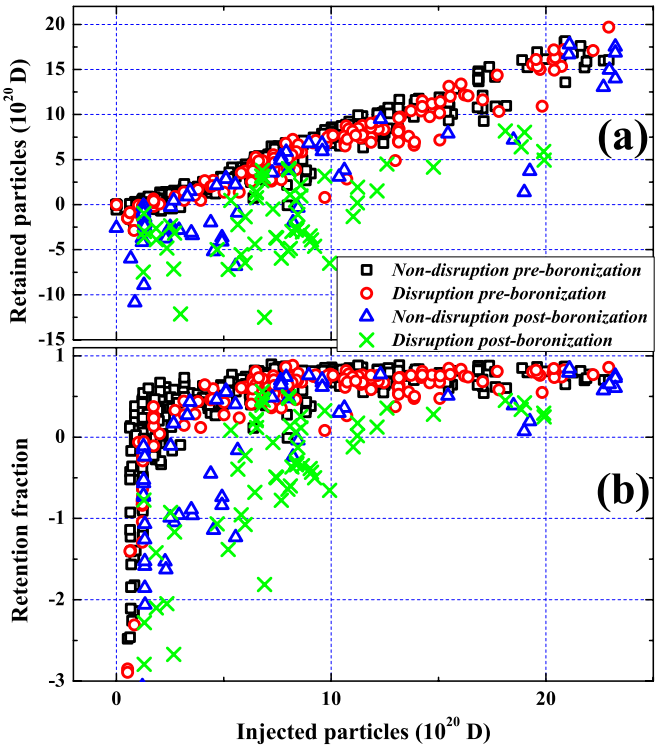

Figure 4. Fuel retention of disruptive and non-disruptive discharges versus injected particles before and after D_2 boronization, (*a*) retained particles and (*b*) retention fraction. Square markers (□) are non-disruptive discharges before boronization, circles (○) are disruptive discharges before boronization, up triangles (△) are non-disruptive discharges after boronization and crosses (×) are disruptive discharges after boronization.

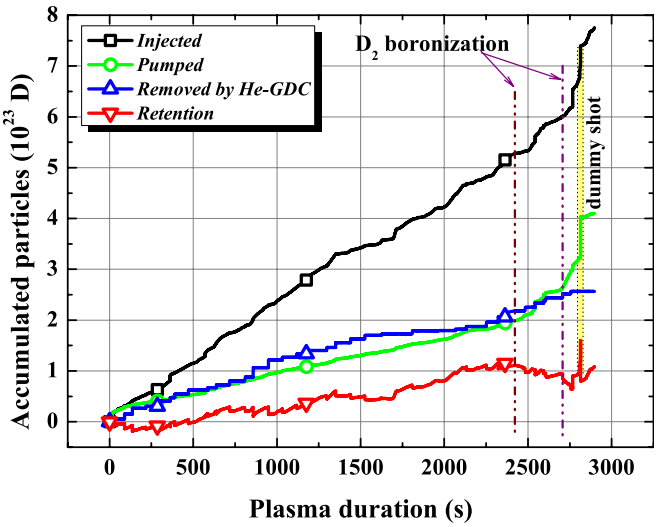

Figure 5. Total accumulated particles of injected (□), pumped between shots (○), removed by He-GDC during night and early morning (△), and retained (▽) in the whole KSTAR 2010 campaign, as a function of accumulated plasma duration. All shots including dummy shots are included in the figure. Deuterium retention during D_2 GDC/boronization is not included in the particle balance due to the lack of measurement. Dashed–dotted lines show the D_2 boronizations, and the steep increase in pumped particles in the yellow region is from consecutive dummy shots.

increases with the number of injected particles. During the shots with low gas injection or shots after D_2 boronization, the retention decreases even down to negative. In these shots, the plasma density is mainly maintained by fuel recycling, i.e. natural density [2], thus the retention is very small during the discharges. If the discharge is disruptive, more particles are desorbed from the wall at the end of discharges, thus the total retention becomes negative. With high gas injection ($>1.2 \times 10^{20}$ D) before the first D_2 boronization, fuel retention is increased as the amount of gas injection increases, and the retention fraction is ~50–90% with different gas injection and plasma parameters. There is no global negative retention (the total amount of gas exhausted in 600 s after the discharge > the total amount of gas injection) observed before the first D_2 boronization even with very high gas injection (18×10^{20} D). And zero or negative retention rate is usually observed only during the phase with low or no gas puffing. These results are very consistent with the results in JET [24] and AUG [25] when they were carbon wall: the fuel retention ratio is increased with the increase in gas puffing, and negative retention occurs at a very low or zero gas puffing.

The deviation of the retained particle number in figure 4(*a*) after the first D_2 boronization is much larger than that before the first D_2 boronization, and many disruptive discharges after the boronization show negative retentions (symbol ×). This indicates that the retention is strongly influenced by hydrogenic particle inventory in boron films shot to shot. Nevertheless, deuterium retention increases with the number of injected particles, even in disruptive shots (section 3.5).

3.3. The effect of wall conditionings on fuel retention

3.3.1. Fuel accumulation and removal by He-GDC. He-GDC is usually carried out after plasma operation of a day during the night and early in the morning before plasma operation. The RGA on KSTAR cannot distinguish D_2 from He, but He injection is at a constant flow rate, therefore the increment of AMU4 pressure by glow plasmas can be taken as D_2 outgassing, and this approximation leads to a removal rate of $\sim 3.5 \times 10^{17}$ D s^{-1} (including D_2 and D atoms in HD). Usually the He-GDC is carried ~5 h at night and 1 h in the early morning (four days with overnight He-GDC, ~14 h), thus the removed deuterium between run days by He-GDC is $\sim(0.5\text{–}1) \times 10^{22}$ D. The long-term outgassing rate during vacuum pumping at night is very small ($\sim 7 \times 10^{15}$ D s^{-1}). Therefore, the total recovered deuterium in both He-GDC and vacuum pumping between two run days is $\sim(0.5\text{–}1) \times 10^{22}$ D, which is usually smaller than the total retention in a run day $\sim(0.7\text{–}3) \times 10^{22}$ D.

Figure 5 shows the overall particle balance in the 2010 campaign: injected, pumped between shots, removed particles by He-GDC at night and early morning, and accumulated retention. All shots including dummy shots are accumulated in figure 5. It is clearly seen that the total retention increases as a function of plasma operation time. At the beginning of the campaign there is negative retention due to frequent D_2-GDC for wall conditioning, which is not included in the particle balance calculation (we have set the 'zero retention' as the first shot of the campaign). Since D_2 boronization has a

strong effect on wall condition, the behavior of He-GDC should be focused on the experiments before the D_2 boronization (dashed–dotted lines in figure 5). It is observed that from the first shot of the campaign to the last shot just before the first D_2 boronization, the total injected, pumped between shots, removed by He-GDC and accumulated retention are 5.3×10^{23} D, 2.0×10^{23} D, 2.2×10^{23} D and 1.1×10^{23} D, respectively. Note that the total number of removed particles by He-GDC is almost equivalent to that pumped between shots, and both of them have very strong effects on fuel recovery from the wall (38–42%); one of the reasons might be the short-pulse plasmas in KSTAR 2010, since the particle balance in short-pulse plasmas is dominated by dynamic retention, and they can be recovered by He-GDC, as mentioned in [1, 2, 11]. Long-term retention (2372 s plasmas before the first D_2 boronization) is 1.1×10^{23} D, i.e. ~21%. Since the retention via implantation is limited to $\sim 10^{21}$ D m^{-2}, which is equivalent to $\sim 5.4 \times 10^{22}$ D in KSTAR, it is lower than the accumulated particles during the whole campaign. Therefore, the long-term retention in KSTAR with a full graphite wall is via co-deposition rather than implantation, which is similar to the results in other tokamaks with a graphite wall [2], while the retention via implantation is expected to be partially removed by He-GDC.

Comparing discharges just after He-GDC with that at the end of the day, morning discharges require more gas injection to maintain a similar plasma density to that at the end of the day. Figure 6 shows four shots with the same plasma current and gas puffing (before 2.5 s). They all are circular ohmic and limiter shots of two successive days. Shot #3311 is at the end of the experiment day, and shots #3319, #3322 and #3334 are on the next experiment day. 3 h night He-GDC and ~1 h next early morning He-GDC are carried out between the two run days. Shot #3319 is the second successful shot of the run day, before which there are 2.5 h vacuum pumping after the morning He-GDC, and shot #3334 is at the end of the run day.

It is observed that shot #3319 has a higher plasma inventory and higher He II emission than all the other three shots, as shown in figures 6(*c*) and (*e*), which indicates the strong helium outgassing from the first wall just after He-GDC. However, the helium outgassing is decreased quickly after three shots, as shown in shot #3322 (He II), which means that the amount of helium retained on the first wall during He-GDC is relatively small, and they can be easily removed by vacuum pumping and several discharges. This confirms the above assumption that He fraction can be negligible in the particle balance analysis. The plasma inventory of shot #3322 is obviously lower than shot #3311 with the same amount of gas injection, and H_α/D_α emission is also lower. It could be attributed to the He-GDC, which recovers the retained deuterium from the first wall, and thus decreases the wall outgassing. As a result, the wall pumping capability is improved, which can be observed from the retention rate during the gas puffing phase: the retention rate in shot #3322 (average 3.5×10^{20} D s^{-1}) is slightly higher than that in shot #3311 (average 3.2×10^{20} D s^{-1}). Moreover, shot #3334 has a similar plasma inventory and retention rate as shot #3311, both due to the accumulation of deuterium retention in the first wall during each run day, which leads to an increased outgassing rate of deuterium, thus a decreased wall pumping capability. Note that the difference in the retention rates of shots in figure 6(*f*) is small compared with that of the plasma inventory shown in figure 6(*c*), indicating that wall pumping capability would be decreased during the day, but only slightly. Combining this fact together with the results in figure 4, it can be deduced that the retention rate is strongly correlated with the amount of injected gas: the same amount of gas injection leads to very similar retention rates for the three different shots. Therefore, higher plasma inventory of shots at the end of the day is thus due to the higher outgassing rate of fuel accumulated during the run day under a relatively constant retention rate.

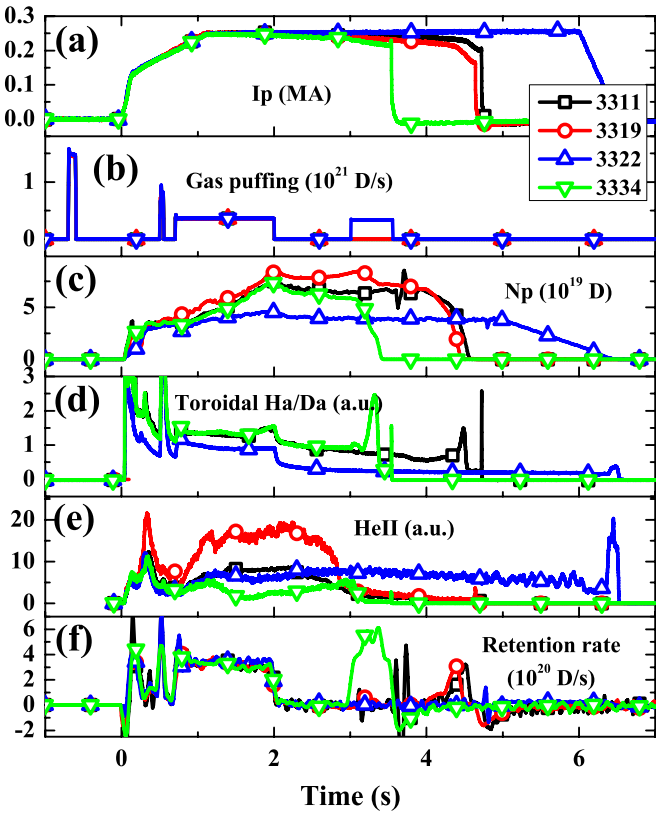

Figure 6. Fuel accumulation in one day and its removal by He-GDC, (*a*) plasma current, (*b*) gas puffing rate, (*c*) plasma inventory (~ proportional to n_e), (*d*) toroidal central H_α/D_α, (*e*) He II emission and (*f*) retention rate. Shot #3311 (square □) is close to the end of one run day, the other three shots are on the next run day. Shot #3319 is the second successful shot of the next run day, shot #3222 (upper triangle △) is the fifth successful one and shot #3334 (down triangle ▽) is close to the end of that run day.

3.3.2. The effect of D_2 boronization on fuel retention. Boronization in KSTAR is carried out using evaporated carborane ($C_2B_{10}H_{12}$) in the D_2 glow discharge. D_2 is used as the carrier gas instead of helium in order to reduce the amount of hydrogen in the boron film and inside the vacuum vessel. ~2–5 h of He-GDC is carried out after the boronization until the RGA levels of hydrogen/deuterium return to the value before the boronization process. Figure 7 shows the number of accumulated deuterium particles as a function of time for 6 run days from 5 to 13 November. The wall inventory is set to zero before the first shot of each day. Wall conditioning during these

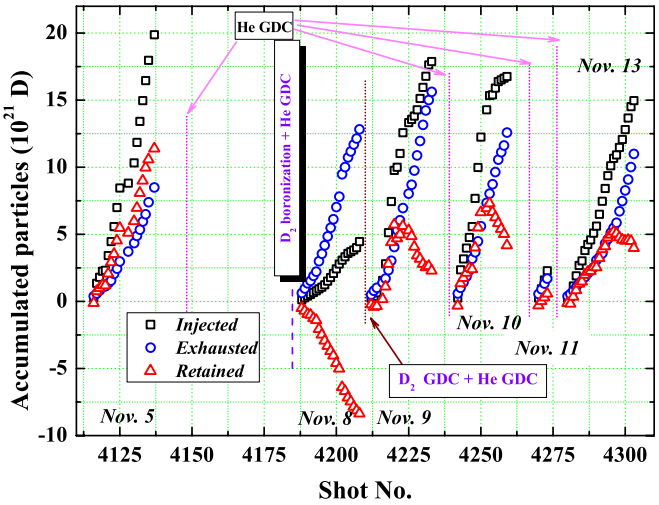

Figure 7. Accumulated particles shot by shot from the first shot of each run day, squares (□) are the injected particles, circles (○) are the exhausted and up triangles (△) are the retained. The data of the run day before boronization are lost due to measurement error, GDC (vertical dotted lines) is carried out at the night and early morning of every day.

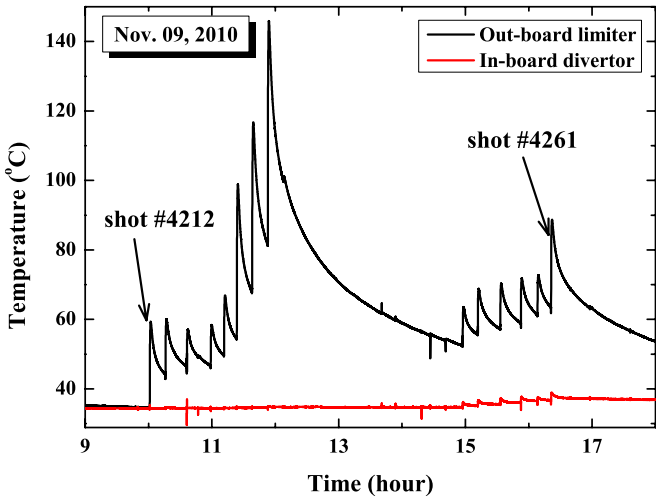

Figure 8. Time evolution of the first wall temperature on 15 November 2010, measured by thermocouples at 5 mm behind the graphite surface. The line with squares (□) is the temperature at the lower in-board limiter, and that with circles (○) is that at the lower in-board divertor. The first and last plasma discharges are shot #4311 and shot #4335, respectively.

days is as follows: 8 November night with D_2-GDC + He-GDC to decrease the hydrogen fraction in the boron film, other days with He-GDC at night for ∼ 2 h and next early morning for ∼1 h. Before the boronization (label Nov. 5), the number of accumulated particles increases as a function of time and reaches ∼1.2 × 10^{22} D at the end of the day. As we have seen above, the average fuel retention is ∼10^{20}–10^{21} D/shot depending on the amount of injected gas. In contrast, strong outgassing of deuterium is observed during the first day after the boronization (label Nov. 8). All shots show a net release of deuterium, and the total amount of release is ∼8.4×10^{21} D, and the number of exhausted particle is 2.5 times higher than that of injected gas. From the second day, first one or two shots show release of particles (mainly helium rather than deuterium due to the morning He-GDC). Afterwards, wall pumping is observed in the initial 12–18 shots with maximum retention up to 83%, and then the total amount of gas exhausted in 10–15 min after the discharge is larger than that of the total injected gas, i.e. long-term wall characteristic becomes puffing from pumping.

This enhanced wall puffing is mainly for two reasons, (a) the wall inventory increases shot by shot, and (b) the wall temperature also increases shot by shot, as shown in figure 8 (higher temperature on the out-board limiter than the divertor region, because plasmas are limiter-type dominant on that day). However, the shots needed to achieve this global negative retention are increased day by day, indicating the gradual recovery of the wall condition. More importantly, the wall still acts as a pump during the gas puffing into the plasma during the discharge, and a part of the injected particles are retained on the first wall, but after the discharge, due to the increased outgassing rate by the higher wall inventory and higher wall surface temperature, the amount of deuterium recovered in 10–15 min after the discharge is larger than the total injected particles. In the case of discharges with only pre-filling, wall puffing (negative retention) is observed during the plasma start-up and during H-mode. A negative retention rate is only observed in the discharges without gas puffing after the plasma start-up, due to its dependence on the gas puffing rate [26].

3.4. Fuel retention in different discharges

3.4.1. Fuel retention in a diverted H-mode discharge. A typical H-mode diverted discharge is obtained by ECRH and NBI after the first D_2 boronization, and four different phases are observed as marked (1)–(4) in figure 9. For more clear understanding, the plasma shapes from EFIT at 0.5, 1.1, 1.5 and 2.5 s, which correspond to the dashed lines in figure 9, are shown in figure 10. The divertor particle flux and the inner limiter particle flux are measured by a fixed Langmuir probe array (their locations are marked as red dots in figure 10). (1) After the plasma ignites, the plasma density increases with a low and steady gas puffing rate of 5.7×10^{20} D s^{-1}. The plasma is in circular shape, as shown in figure 10(*a*). In this phase the retention rate decreases from 6×10^{20} D s^{-1} at the beginning of gas puffing at 0.2 s, to a low value of 0.7 × 10^{20} D s^{-1} at 0.7 s, which means that the wall seems to be close to an implantation saturation status under this low gas puffing condition. (2) When the gas puffing is stopped, the retention rate quickly becomes negative, due to the outgassing from the outer limiter where the plasmas strongly impact, as shown in figure 10(*b*). When the plasma is elongated and reaches the divertor region, as observed from the increase in particle flux to the divertor in figure 9(*e*) and divertor H_α/D_α emission in figure 9(*f*), a sharp increase in the retention rate resulting from a strong retention in the divertor region is obtained. (3) After the L–H mode transition, the plasma is fully attached to the divertor, as shown in figure 10(*c*). Both the plasma stored energy and plasma density (almost proportional to N_p) are increased notably, as shown in figures 9(*a*) and (*c*). After a peak retention rate during the L–H transition, the retention rate quickly decreases to negative, which results from (a) fuelling is stopped before the L–H transition, inducing a decreased retention since retention

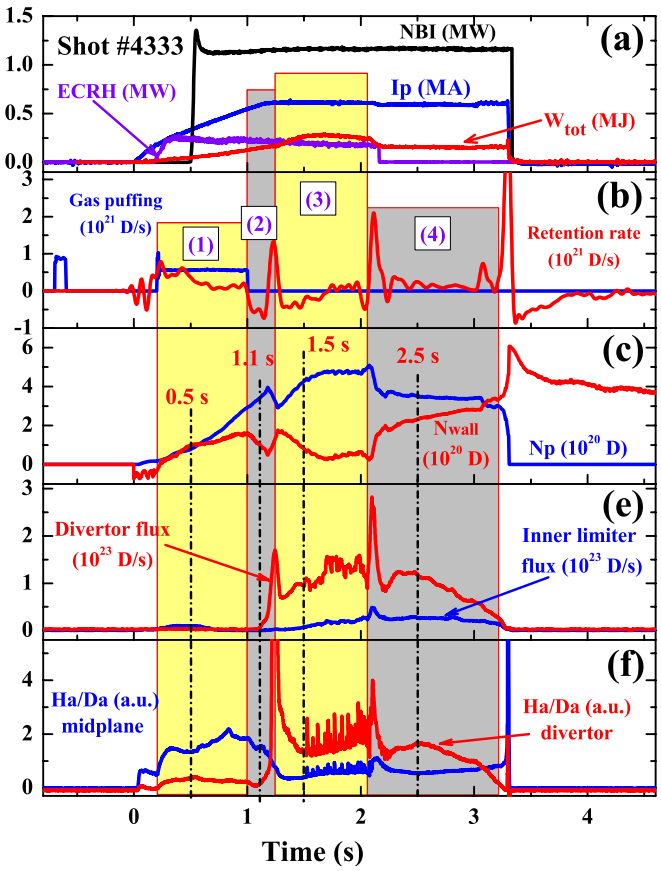

Figure 9. Time evolution of plasma parameters of divertor H-mode shot #4333, (*a*) plasma current (blue), ECRH power (purple), NBI power (black) and plasma stored energy (W_{tot}, red), (*b*) gas puffing rate (blue) and retention rate (red), (*c*) plasma inventory (N_p, blue) and wall retention (N_{wall}, red), (*d*) inner limiter particle flux (blue) and divertor particle flux (red), and (*f*) toroidal central (blue) and divertor H_α/D_α (red, figure 10 shows its poloidal position).

is strongly affected by the gas puffing rate, and (b) the increase in particle confinement in H-mode decreases the particle loss from the plasmas, while the recycling particles from the wall may be similar, thus the retention rate is decreased further. After that, a balance between wall pumping and wall puffing is reached, the average retention rate is very small, almost close to zero, as shown in figure 9(*b*). The negative retention at the initial phase of H-mode and the very low retention rate after that are also observed in other tokamaks [5]. (4) The H–L mode back-transition leads to a decrease in plasma inventory to almost that before the L–H mode transition, and the decrease in plasma confinement causes a higher particle flux from the plasma to the first wall, as in figure 9(*e*), resulting in a higher retention rate, as shown in figure 9(*b*). During the ramp-down, most of the plasmas are temporarily retained on the wall and then they are released after the discharge, as mentioned in section 3.1.

The divertor particle flux during H-mode ($\sim 1.5 \times 10^{23}$ D s^{-1}) is much higher than both the gas injection rate and the retention rate. Moreover, the time evolution of divertor particle flux is similar to the divertor H_α/D_α, which indicates the strong recycling in the divertor region, and the net retention (ΔN_{wall}) during the whole H-mode phase is negative, as shown in figure 9(*c*), which might be attributed to (1) a decreased total particle flux to the wall by the enhanced particle confinement during H-mode, (2) no gas puffing and (3) probably implantation saturated divertor wall by the strong particle flux (10^{23} D s^{-1}) during previous divertor discharges. When the plasmas transit back to the L-mode, the increased particle flux on the inner limiter and decreased one on the divertor are due to the change in plasma shape and position. As shown in figure 10(*d*) at 2.5 s, the plasmas are limited by the inner wall inducing a strong particle flux to the inner limiter, while the X-points are a little far away from both upper and lower divertors, which decreases the particle flux to the divertor.

3.4.2. Deuterium release by ECRH heating. Wall outgassing and edge plasma density increased by ECRH are observed in HL-2A [27]. A similar observation is made in KSTAR: the plasma density increases with ECRH injection without additional particle injection in circular and limiter plasmas. Figure 11 shows two successive discharges with and without ECRH heating, while other parameters such as gas puffing, plasma shape and plasma current are identical, and there is no additional gas puffing after the plasma start-up. In shot #3859, the plasma density is increased immediately when ECRH is injected, as shown in figure 11(*b*), and toroidal H_α/D_α (central channel) emission is also enhanced after ECRH injection in figure 11(*f*). Moreover, neutral pressure with ECRH heating in shot #3859 is higher than that in shot #3860 without ECRH, as shown in figure 11(*d*), which obviously indicates the enhanced wall outgassing by ECRH. The wall inventory calculated by particle balance is shown in figure 11(*g*). It can be seen that wall retention is significantly lower in shot #3859 after the ECRH injection than that in shot #3860 without ECRH, and the maximum difference between the two shots is $\sim 4.8 \times 10^{19}$ D. The increase in the plasma density and decreased retention by ECRH are probably due to the direct deposition of ECRH power on the first wall, which causes enhanced wall outgassing [28, 29]. With constant ECRH injection, the plasma density decreases due to the density pump-out effect of ECRH [30], consequently neutral pressure and wall retention increase slightly. As the ECRH is turned off in shot #3859, H_α/D_α decreases immediately, and there is a very slight and slow decrease in the plasma density and neutral pressure, and the wall retention shows a similar behavior, as shown in figure 11(*g*). At the end of the flattop, the characteristics of both shots are almost the same, which clearly indicates that the effect of ECRH on retention is only temporary. Figures 11(*b*) and (*g*) also show that the effect of ECRH on retention at the end of ECRH is not as strong as that at the beginning of ECRH heating, probably due to the decreased outgassing rate by the constant ECRH power deposition on the local wall surface.

3.4.3. Deuterium recovery in different discharges. Experimental data show that the variation of the exhausted particle number due to different injection and/or plasma parameters is small, usually within a factor of 2 [2], and disruptions release more particles than non-disruptions, as

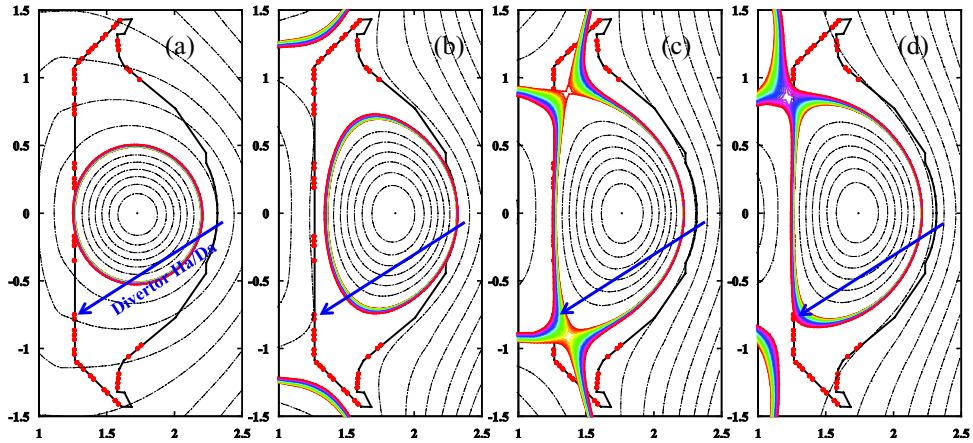

Figure 10. EFIT result of shot #4333, with emphasized SOL position by color contours, at (*a*) 0.5 s, (*b*) 1.1 s, (*c*) 1.5 s and (*d*) 2.5 s. Red dots are the Langmuir probes, blue line with an arrowhead represents the poloidal position of one channel divertor H_α/D_α, corresponding to figure 9(*f*).

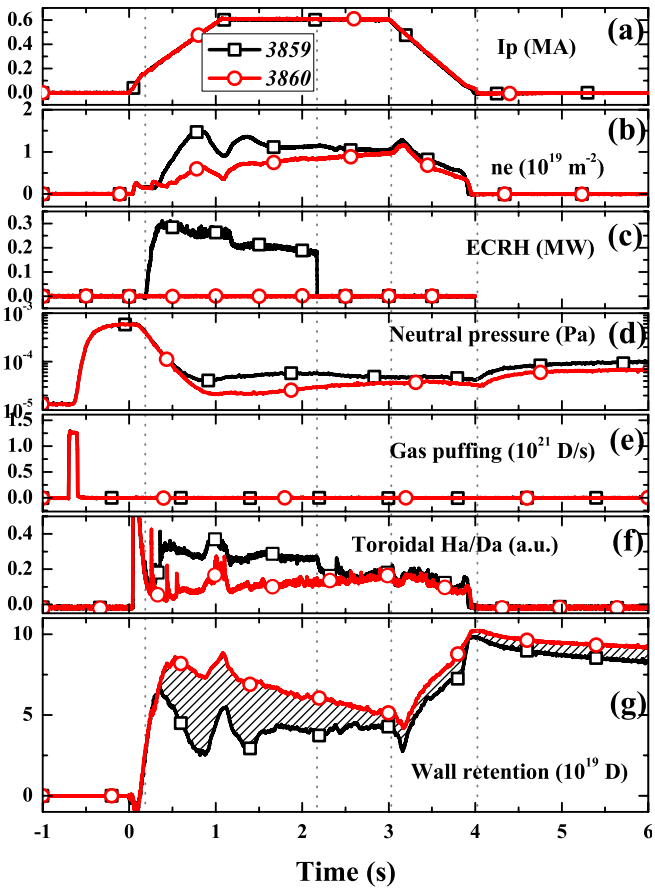

Figure 11. Influence of ECRH on fuel retention in shot #3859, square (□), and shot #3860, circle (○), (*a*) plasma current, (*b*) line integral density (n_e), (*c*) ECRH power, (*d*) neutral pressure, (*e*) gas puffing rate, (*f*) toroidal central H_α/D_α emission and (*g*) wall retention.

observed in JET [12], Tore Supra [31], Alcator C-mod [32] and DIII-D [33]. During the disruption, large thermal energy is deposited directly on the first wall, which causes a rapid increase in the surface temperature to a high value, therefore more particles are released by the thermal desorption process. During the KSTAR 2010 campaign, the amount of recovered deuterium after discharges is in a wider range of (1–11) × 10^{20} D-atoms than that in the [2], which is due to the large range of plasma parameters (different plasma current, shape, wall temperature, amount of gas injection and so on).

Figure 12 shows three different shots: a normal discharge with good plasma current start-up and ramp-down (shots #4212), a disruptive shot (shot #4213) with a current quench rate of 41 MA s^{-1} and a failed shot (shot #4215) with gas breakdown but failed current ramp-up at 160 kA. They all are after D_2 boronization and limiter discharges; neither ECRH nor NBI is used. Only pre-filling via a piezoelectric valve is used for gas puffing. The retention rate has a peak at the plasma start-up for all the three shots, as shown in figure 12(*d*), and most pre-filling particles are retained to the first wall during the plasma start-up in figure 12(*e*). With the increase in plasma inventory after the plasma breakdown in shots #4212 and #4213, the wall retention is decreased along with an increase in plasma density. At the end of the two discharges, similar to shot #3643 as mentioned above, most plasma particles impact on the first wall and stay on the wall for a while. After that a part of them are desorbed from the wall. For the disruptive shot #4213, the neutral pressure increase is higher than the non-disruptive shot #4212 in figure 12(*c*), and also the retention rate shows a stronger outgassing (negative retention rate) after the plasma terminates in shot #4213 than that in shot #4212, as shown in figure 12(*d*). As a consequence, wall retention in shot #4213 decreases significantly in figure 12(*e*). However, shot #4215 is quite different from the other two shots discussed above: the plasma is terminated during the plasma start-up at a very low plasma density ($N_p \sim 1.5 \times 10^{19}$ D) and low plasma current (160 kA). No strong pressure increase after that due to the outgassing is observed, and the outgassing rate is quite low compared with the other two shots, from 3.4×10^{19} during 0–20 s after the plasma terminates, to 5.4×10^{16} after that. This indicates that a very limited amount of deuterium is recovered from the first wall in shot #4215, which is probably due to the low plasma current and density, and consequently restricted thermal release of deuterium. The numbers of recovered particles after each discharge in 600 s from shots #4212, #4213 and #4215 are 2.0×10^{20}, 2.3×10^{20} and 1.5×10^{20} D,

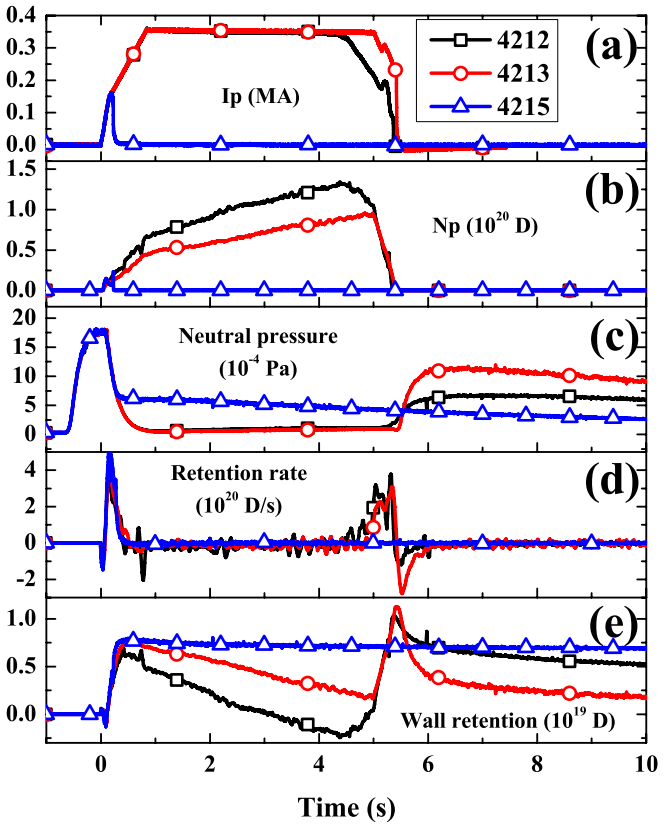

Figure 12. Deuterium retention and recovery after discharges with different plasma parameters, (*a*) plasma current, (*b*) plasma inventory, (*c*) neutral pressure, (*d*) retention rate and (*e*) wall retention. Square markers (□) show shot #4212 with good plasma start-up and soft-landing, circles (○) show shot #4213 whose parameters are similar to shot #4212 but with a disruptive end, up triangles (△) show shot #4215 with gas breakdown but plasma current ramp-up fails at 160 kA.

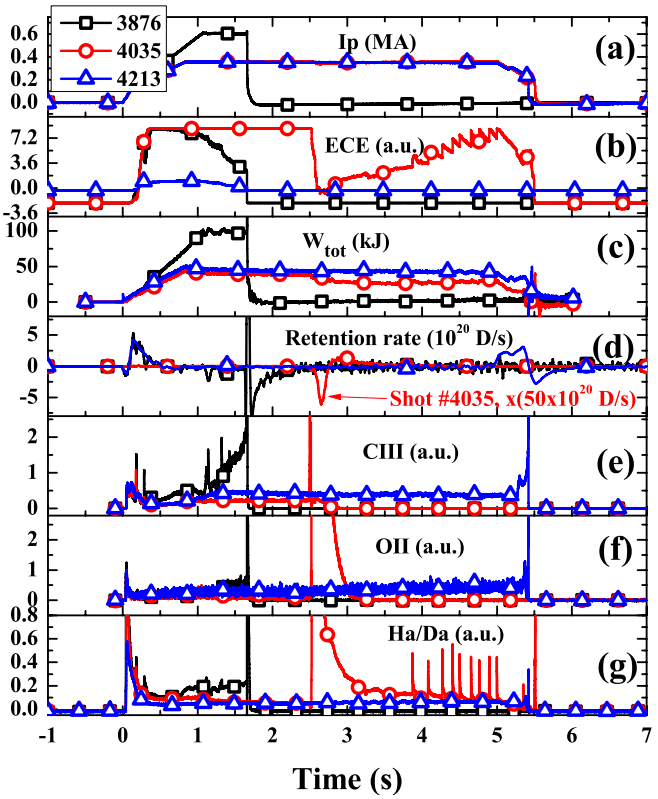

Figure 13. Deuterium recovery and impurity radiation in different disruptive shots: #3876 square (□), #4035 circle (○) and #4213 up triangle (△); (*a*) plasma current, (*b*) central electron temperature measured by ECE, (*c*) plasma stored energy (W_{tot}), (*d*) retention rate, for shots #3876 and #4213 it is in 10^{20} D s^{-1}, but for shot #4025 it is in 50 × 10^{20} D s^{-1} due to its much large scale, (*e*) C III radiation, (*f*) O II radiation and (*g*) toroidal central H_α/D_α emission.

respectively. (The total number of injected particles of the three shots is the same, 1.2 × 10^{20} D, which is lower than the number of recovered particles. The negative retentions of these three shots are due to the wall-loaded D_2 during the D_2 boronization.)

Disruptive shots with a large plasma stored energy (W_{tot}) and a high quench rate would release much more gas from the first wall than shot #4213 mentioned above. Shot #3876 is a major disruption with a current quench rate of 71 MA s^{-1} under $B_T = 2$ T. A plasma stored energy of ∼100 kJ is suddenly deposited onto the first wall in 5 ms during the disruption, CCD and H_α/D_α data show that the plasma mainly impacts the inner limiter at the disruption. After the disruption, a large outgassing rate (negative retention rate) is observed, as shown in figure 13(*d*). The total amount of D released after the disruption in 600 s is ∼2.8 × 10^{20} D, which is 2.3 times higher than that of particle injection (1.2 × 10^{20} D). Strong desorption of other impurities is also observed, including H_2O, CO, CO and hydrocarbons. Comparing shot #4035 with other major disruptions, it is seen that shot #4035 is a very unique 'disruption'. In the middle of the discharge the plasma confinement is destroyed by the deep injection of FRP (with graphite shield), which causes a strong plasma–material interaction. Strong erosion/outgassing from the graphite shield leads to an increase in the plasma density by a factor of ∼9, and the peak neutral pressure is three orders of magnitude higher than that before the FRP injection. The RGA shows that most of the released gases are CO, CD_4 and D_2 (not shown here). The impurity radiation of C III and O II (edge), and H_α/D_α (toroidally central channel) emission are all increased, as shown in figures 13(*e*)–(*g*). The increase in the emission intensity of the impurity species is instantaneous. Surprisingly, the plasma is survived with almost the same plasma current. Both the plasma density and neutral pressure are decreased gradually until the plasma is terminated. The C III line intensity is decreased quickly while those of O II and H_α/D_α return slowly to their original values. The released particles are retained on the wall again by the survived plasmas, which can be considered as the additional gas injection into the plasmas, and the total gas recovered after the discharge in 600 s is 1.3 × 10^{20} D, which is only ∼4% of the amount of gas recovered from the disruption in the middle of this shot.

3.5. Discussion on correlation between pulse length and retention rate

In the KSTAR 2010 campaign, all discharges are less than 7 s. No feedback density control is employed. Figure 14 shows the correlation between average retention rates (integrated total retention divided by the discharge pulse length) before

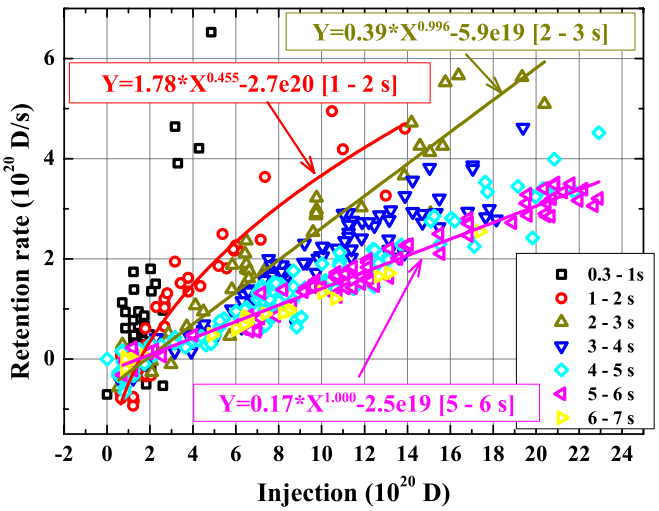

Figure 14. Retention rate of discharges before D_2 boronization with different pulse lengths and injected particles, square (□) is 0.3–1 s, circle (○) is 1–2 s, up triangle (△) is 2–3 s, down triangle (▽) is 3–4 s, diamond (◇) is 4–5 s, left triangle (◁) is 5–6 s and right triangle (▷) is 5–7 s. The three lines are power law fittings for 1–2 s (red), 2–3 s (dark yellow) and 5–6 s (pink).

D_2 boronization at different pulse lengths and the number of injected particles. In all cases, the retention rate increases as a function of the number of injected particles. As the pulse length increases, the gradient of retention rate decreases indicating that the retention decreases. In other words, particle release (outgassing) from the wall increases due to the increase in wall temperature (increase in plasma–wall interaction time). The first wall temperature evolution of one day is shown in figure 8; the temperature is increased notably shot by shot. Moreover, the power law fitting result shows that, in the short-pulse discharges (1–2 s), the retention rate increases as the number of injected particles with a low increasing ratio of 0.445, the increasing ratio is increased to 0.996 in shots with pulse lengths of 2–3 s, and in shots with pulse lengths of 5–6 s it is almost 1, i.e. the retention rate increases linearly as the amount of gas injection, as shown in figure 14. As the pulse length increases, the retention rate converges after 4 s of pulse length because their increasing ratio is larger than 0.9, they all almost linearly increase with particle injection. The maximum average retention rate is 6.5×10^{20} D s^{-1} with a pulse length of 0.43 s, and the retention rates of most shots are in a wide range of $(0.2–6) \times 10^{20}$ D s^{-1}. In the KSTAR 2010 campaign, all discharges are non-steady state short pulse with a duration of less than 7 s. From figure 14 it is clearly seen that the retention rate increases with the injection amount but decreases with the pulse length. Therefore, it would be expected that, when steady-state long-pulse plasmas are achieved in KSTAR, the retention rate would show a linear response to the number of injected particles with the lowest gradient in figure 14 (the same behavior as Tore Supra, 2×10^{20} D s^{-1} [34]).

4. Conclusions

In the KSTAR 2010 campaign with a full graphite first wall, particle balance is employed to comprehensively investigate fuel retention and release with different plasma parameters. From the typical retention evolution during the discharge, it is observed that the dominant retention occurs during the gas puffing into the plasmas. The number of retained deuterium particles increases with the number of injected particles in both disruptive and non-disruptive discharges. Before the boronization assisted by a D_2 glow discharge, most shots with a large number of injected particles ($>1.2 \times 10^{20}$ D) have high retention fractions up to ~50–90% even in disruptive discharges, and negative retention (the total number of exhausted particles in 600 s after discharges > that of injected) is only observed in shots with a small number of injected particles ($<8 \times 10^{19}$ D). Deuterium retention accumulation in the first wall decreases the wall pumping capability, and He-GDC at night and early morning is effective in recovering the wall pumping capability. From the global particle balance in the whole campaign including the recovered deuterium in He-GDC, it can be concluded that retention via implantation can be partially recovered by He-GDC, and long-term retention is via co-deposition. D_2 boronization strongly enhances the wall puffing and leads to a negative retention. But the wall pumping capability is recovered in 2–3 days by night and early morning He-GDC.

Comparing the retention in different discharges, ECRH enhances wall outgassing during the discharge, but the outgassed particles are retained on the wall again if the ECRH is stopped before the plasma terminates, thus its effect on global retention is very weak. During diverted H-mode discharges, the retention rate decreases to zero or even negative, which is similar to other tokamaks. Moreover, the divertor particle flux is $\sim 1.5 \times 10^{23}$ D s^{-1}, which is much higher than the retention rate, indicating the strong recycling divertor. The amount of recovered deuterium from the wall after discharges is dependent mainly on the plasma–wall interaction when the plasma is terminated, and disruptive discharges release more particles from the first wall, especially the disruptions with a large plasma energy and a high quench rate.

Acknowledgments

This study is supported by the Korean Ministry of Education, Science and Technology under the KSTAR project. The authors would like to thank the members of the KSTAR team, who gave valuable contributions to the experiments, especially during the piezoelectric valve and pumps calibration and data acquisition. The authors would also like to specially thank Dr Alan England for technical discussions.

References

[1] Federici G *et al* 2001 *Nucl. Fusion* **41** 1967–2137
[2] Loarer T *et al* 2007 *Nucl. Fusion* **47** 1112–20
[3] Loarer T 2009 *J. Nucl. Mater.* **390–391** 20–8
[4] Roth J *et al* 2008 *Plasma Phys. Control. Fusion* **50** 103001
[5] Unterberg E A *et al* 2011 *J. Nucl. Mater.* **415** S740–7
[6] Hu J S *et al* 2005 *Plasma Phys. Control. Fusion* **47** 1271–86
[7] Loarer T *et al* 2004 *31st EPS Conf. on Plasma Phys. (London, UK)* vol 28G (ECA) P-1.139
[8] Sakamoto M *et al* 2004 *Nucl. Fusion* **44** 693–8

[9] Houtte D van *et al* 2004 *Nucl. Fusion* **44** L11–15
[10] Nakano T *et al* 2007 *J. Nucl. Mater.* **363–365** 1315–22
[11] Huang J *et al* 2010 *Plasma Phys. Control. Fusion* **52** 075012
[12] Philipps V *et al* 2009 *J. Nucl. Mater.* **390–391** 478–81
[13] Rohde V *et al* 2009 *J. Nucl. Mater.* **390–391** 474–7
[14] Tsitrone E *et al* 2011 *J. Nucl. Mater.* **415** S735–9
[15] Kwon K *et al* 2011 *Nucl. Fusion* **51** 094006
[16] Bak J G *et al* 2011 *15th ITPA Meeting on SOL/Divertor Physics (Helsinki, Finland)*
[17] Yu I K *et al* 2008 *Fusion Eng. Des.* **83** 117–22
[18] Seo S H *et al* 2008 *Rev. Sci. Instrum.* **79** 116103
[19] Kubo H *et al* 2006 *Proc. of 21st Int. Conf. on Fusion Energy (Chandu, China)* http://www-naweb.iaea.org/napc/physics/fec/fec2006/papers/ex_p4-11.pdf
[20] Tsitrone E *et al* 2002 *Plasma Phys. Control. Fusion* **44** 701–15
[21] MAINGI R *et al* 1996 *Nucl. Fusion* **36** 245–53
[22] Ogiwara N *et al* 1990 *J. Vac. Sci. Technol.* A **8** 3855–63
[23] ITER Physics Basis Chapter 3 1999 *Nucl. Fusion* **39** 2251–389
[24] Loarer T *et al* 2003 *30th EPS Conf. on Controlled Fusion and Plasma Physics (St Petersburg, Russia)* vol 27A (ECA) P-1.161
[25] Mertens V *et al* 2003 *30th EPS Conf. on Controlled Fusion and Plasma Phys. (St Petersburg, Russia)* vol 27A (ECA) P-1.128
[26] Asakura N 2004 *Plasma Phys. Control. Fusion* **46** B335–47
[27] Zou X L *et al* 2010 *23rd IAEA Fusion Energy Conf. (Daejeon, Korea)* EXC/P8-20
[28] Vershkov V A *et al* 1991 *Plasma Phys. Control. Fusion* **33** 1235
[29] Hartfuss H J *et al* 2003 *30th EPS Conf. on Controll Fusion and Plasma Phys. (St Petersburg, Russia)* vol 27A (ECA) O-3.2C
[30] Zushi H *et al* 1996 *Plasma Phys. Control. Fusion* **38** 1307–12
[31] Pégourié B *et al* 2011 *J. Nucl. Mater.* **415** S809–12
[32] Whyte D G *et al* 2006 *Proc. 21st Int. Conf. on Fusion Energy (Chengdu, China)*
[33] Hollmann E M *et al* 2009 *J. Nucl. Mater.* **390–391** 597–601
[34] Tsitrone E *et al* 2009 *Nucl. Fusion* **49** 075011